Micropatterning of costimulatory ligands enhances CD4$^+$ T cell function

Keyue Shen*, V. Kaye Thomas†, Michael L. Dustin†, and Lance C. Kam*‡

*Department of Biomedical Engineering, Columbia University, New York, NY 10027; and †Molecular Pathogenesis Program, Skirball Institute of Biomolecular Medicine, New York University School of Medicine, New York, NY 10016

Edited by Arthur Weiss, University of California School of Medicine, San Francisco, CA, and approved March 19, 2008 (received for review October 30, 2007)

Spatial organization of signaling complexes is a defining characteristic of the immunological synapse (IS), but its impact on cell communication is unclear. In T cell–APC pairs, more IL-2 is produced when CD28 clusters are segregated from central supramolecular activation cluster (cSMAC)-localized CD3 and into the IS periphery. However, it is not clear in these cellular experiments whether the increased IL-2 is driven by the pattern itself or by upstream events that precipitate the patterns. In this article, we recapitulate key features of physiological synapses using planar costimulation arrays containing antibodies against CD3 and CD28, surrounded by ICAM-1, created by combining multiple rounds of microcontact printing on a single surface. Naïve T cells traverse these arrays, stopping at features of anti-CD3 antibodies and forming a stable synapse. We directly demonstrate that presenting anti-CD28 in the cell periphery, surrounding an anti-CD3 feature, enhances IL-2 secretion by naïve CD4$^+$ T cells compared with having these signals combined in the center of the IS. This increased cytokine production correlates with NF-κB translocation and requires PKB/Akt signaling. The ability to arbitrarily and independently control the locations of anti-CD3 and anti-CD28 offered the opportunity to examine patterns not precisely attainable in cell–cell interfaces. With these patterns, we show that the peripheral presentation of CD28 has a larger impact on IL-2 secretion than CD3 colocalization/segregation.

costimulation | immunology | naïve T cells | microarrays

Communication between T cells and antigen-presenting cells (APCs) forms a key regulatory point of the immune system, mediated in large part by interactions between cell-surface proteins in a small (≈75 μm^2) intercellular contact area termed the immunological synapse (IS). It is hypothesized that the spatial organization of receptor/ligand complexes within the IS is an important part of the language of T cell–APC communication (1, 2). The archetypical organization of mature synapses consists of a central supramolecular activation cluster (cSMAC) containing TCR/MHC complexes and surrounded by a peripheral (pSMAC) region rich in ICAM-1/LFA-1 clusters; the function of this bull's-eye pattern, as well as alternative geometries, in modulating T cell activation is of much contemporary interest (3–7). Recent studies have also suggested a functional role of microscale organization of CD28 ligation, a classic costimulatory signal, in modulating T cell response. Andres *et al.* (8) showed that during the initial minutes of T cell/APC interaction, CD28 and TCR comigrate, leading to cSMAC localization of both complexes. At later time points, Tseng and colleagues (9) showed that CD28/CD80 complexes segregate from TCR/MHC into either the cSMAC periphery or pSMAC. Surprisingly, truncation of the CD80 cytosolic domain, which reduces T cell activation (10), promoted colocalization of TCR/MHC and CD28/CD80 complexes in the cSMAC (9). Because the modifications to CD80 were in the APC, this result suggests that T cells recognize and respond to micrometer-scale organization of CD28 ligands, particularly with respect to TCR signaling complexes. However, it has been difficult to test this hypothesis further by using T/APC systems.

To gain the required control over IS geometry, we replaced the APC with a planar substrate containing high-density arrays of antigenic and costimulatory signals (Fig. 1*A*). The use of such surfaces to investigate the IS is well established (3, 5, 11, 12). In particular, Doh and Irvine (13) used complementary, two-component patterns of TCR and LFA-1 ligands to modulate the geometry of synapses formed by preactivated T cells, demonstrating that changing the geometry of TCR engagement modifies activation. However, our need to independently control the geometry of TCR and CD28 ligands, against a background of ICAM-1, poses a more complex challenge in surface preparation. We combined multiple rounds of microcontact printing (14–17) on a single substrate, yielding an additive and extensible process that offers arbitrary control over pattern geometry. We demonstrate that naïve CD4$^+$ T cells respond differentially to these patterns, as measured by secretion of IL-2. From this high-level cellular function, we examine the molecular events leading from TCR/CD28 engagement to IL-2 secretion (18, 19) and identify Akt as a key integrator that allows T cells to recognize pattern geometry.

Results

Patterning of Multicomponent Surfaces. To test the hypothesis that microscale organization of TCR and CD28 signaling within a single IS can modulate activation of naïve T cells, we designed two patterns of ligands for the TCR complex and CD28, surrounded by LFA-1. In a "colocalized" configuration (Fig. 1*B*), each synaptic site contains activating antibodies to both TCR (anti-CD3) and CD28 (anti-CD28) in a single 2-μm-diameter feature. The two antibodies were combined in solution and patterned on a surface in a single step; ICAM-1 was subsequently deposited from solution. In a "segregated" configuration (Fig. 1*C*), CD28 engagement is redirected to a set of 1-μm-diameter satellite features; by this design, a typical cell of 6-μm diameter is expected to interact with four satellite features, together presenting the same total stimulation as a single site on the colocalized surface. These three-component surfaces were created by patterning anti-CD3 and anti-CD28 in separate steps of microcontact printing, followed by coating the substrate with ICAM-1. The resultant features showed minimal cross-contamination, as illustrated in Fig. 1*C Inset*. While various implementations of microcontact printing often result in accumulations of proteins along pattern boundaries, our choice of conditions yielded features that dropped off smoothly over ≈500 nm from a uniform, central plateau.

T cell responses depend highly on the surface concentration of

Author contributions: K.S., M.L.D., and L.C.K. designed research; K.S. and V.K.T. performed research; K.S., M.L.D., and L.C.K. analyzed data; and K.S., M.L.D., and L.C.K. wrote the paper.

The authors declare no conflict of interest.

This article is a PNAS Direct Submission.

‡To whom correspondence should be addressed. E-mail: lk2141@columbia.edu.

This article contains supporting information online at www.pnas.org/cgi/content/full/0710295105/DCSupplemental.

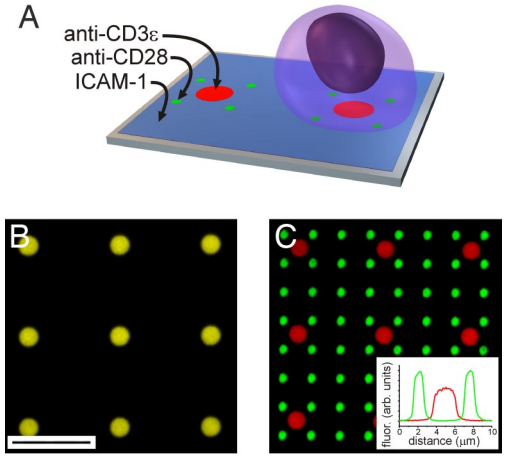

Fig. 1. T cell interaction with micropatterned, costimulatory arrays. (*A*) CD4$^+$ cells were presented with surfaces that capture the microscale organization of ligands associated with T cell costimulation. Colocalized patterns were created by mixing anti-CD3 and anti-CD28 antibodies (yellow) in a single step (*B*), while segregated patterns were defined by sequential patterning of anti-CD3 (red) and anti-CD28 (green) on a single surface (*C*). (*Inset*) Fluorescence profile across a segregated site. ICAM-1 was coated onto the remainder of these surfaces but is omitted here for clarity. (Scale bar: 10 μm.)

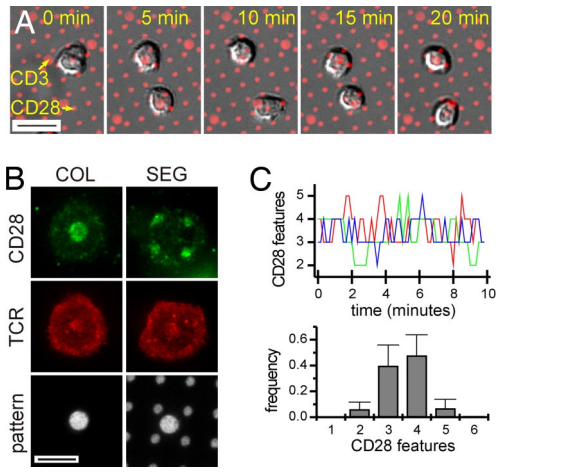

Fig. 2. Interaction of CD4$^+$ T cells with micropatterned arrays. (*A*) In this series of images, features of anti-CD3 (larger, 2-μm dots) and anti-CD28 (smaller, 1-μm dots) are shown in red. Cells were seeded onto surfaces 30 min before collection of this time series. A full movie is shown as Movie S1. (Scale bar: 10 μm.) (*B*) Localization of TCR (detected by using an H57 antibody) and CD28 (antibody against the cytosolic domain) follows the patterned antibodies. (Scale bar: 5 μm.) (*C*) Cells on segregated surfaces interacted predominantly with three or four anti-CD28 features (see text).

ligands. To control this factor, we first measured the surface density of antibodies deposited by microcontact printing. The fluorescence intensity of printed antibodies was quantified by using a series of supported lipid bilayers containing defined amounts of labeled lipids as calibration standards. The plateau of these features corresponded to a density of 200 molecules per μm^2, with a variation of $\approx$15% across different regions of a substrate and between samples (n = 7). This density is a small fraction (<10%) of a close-packed protein monolayer but is in the range required to evoke a costimulatory response and much larger than that needed for effective TCR engagement (11). Surface density was independent of feature size and similar for anti-CD3 and anti-CD28. The surface density of these antibodies was adjusted by dilution with TS2/4 (an antibody that is nonreactive in the context of these experiments) in the coating solution while keeping the total concentration of protein constant. The concentration of patterned antibody, demonstrated for anti-CD3 in supporting information (SI) Fig. S1, varied linearly with dilution with TS2/4; this choice of antibodies is quite fortuitous because we do not expect this linear relation to be universal, given variations in the stamping properties of different antibodies. Our approach was further confirmed on surfaces with "standard" colocalized and segregated patterns defined in the following section; dilution with TS2/4 was used to control the amount of anti-CD3 and anti-CD28 (labeled with Cy5 and Alex 568, respectively) presented to a typical cell. On colocalized surfaces, total fluorescence (arbitrary intensity units $\times$ pixels) associated with each 2-μm feature was $6.9 \times 10^5 \pm 9.8 \times 10^4$ for anti-CD3 and $5.4 \times 10^6 \pm 7.7 \times 10^5$ for anti-CD28 (mean $\pm$ SD, $n > 120$ features; the magnitudes reflect differences in surface concentration, spectra, and camera response). On segregated patterns, the anti-CD3 intensity associated with each 2-μm feature was $7.0 \times 10^5 \pm 7.7 \times 10^4$, similar to the colocalized surface, while that for anti-CD28 on each 1-μm feature was $1.4 \times 10^6 \pm 4.3 \times 10^4$, thus ¼ of that from the larger 2-μm feature on the colocalized pattern, as designed.

T Cell Recognition of Costimulatory Arrays. Naïve CD4$^+$ T cells (>85% purity) were isolated from mouse lymph nodes and seeded onto patterned surfaces. As illustrated in Fig. 2*A* and Movie S1, cells were able to attach to and traverse across these arrays. Cells were predominantly rounded in morphology and slowly motile (1–4 μm/min; upper cell in Fig. 2*A* and Movie S1) as is characteristic for naïve cells (20), although polarized, highly migratory cells (10–20 μm/min; lower cell in Fig. 2*A* and Movie S1) were occasionally observed. Both types of cells halted on anti-CD3 features, typically within the first 30 min of being seeded onto a substrate, similar to the "stop" signal associated with TCR engagement by preactivated T cells observed (13, 21). Cells remained locally active, extending processes away from the anti-CD3 dot but not releasing this feature. Cells were very sensitive to the presence of anti-CD3 and were able to recognize dots as small as 1 μm in diameter and diluted 1:10 (wt/wt) with TS2/4. In contrast to anti-CD3, anti-CD28 did not stop T cell motion, even when patterned at high concentration. We thus established a set of three standard patterns.

- CD3-only (CD3): square array of 2-μm-diameter dots patterned by using a 1:10 dilution of anti-CD3:TS2/4 (2.5 μg/ml:25 μg/ml) and spaced at a 12-μm center-to-center pitch. This control surface reflects TCR signaling without costimulation.
- Colocalized (COL): array of 2-μm-diameter dots patterned by using a 1:10 mix of anti-CD3:anti-CD28 spaced at a 12-μm pitch. This pattern mimics the IS pattern observed with cytoplasmic domain deleted CD80.
- Segregated (SEG): array of 2-μm-diameter dots (12-μm pitch) patterned by using a 2.5 μg/ml:25 μg/ml mix of anti-CD3:TS2/4. This was overlaid with an array of 1-μm-diameter dots of anti-CD28 (25 μg/ml) spaced at a 4-μm pitch. This mimics the IS pattern observed with intact CD80.

TCR and CD28 localization closely reflected the patterns of anti-CD3 and anti-CD28 (Fig. 2*B*, collected 30 min after cell seeding), indicating that these surfaces were effective at directing receptor ligation. Interaction with the segregated pattern was further characterized by counting the number of anti-CD28 features that cells contacted. Two hours after seeding, the cell–substrate interface was observed by interference reflection microscopy at 10-sec intervals over a period of 10 min; these footprints, which were slightly smaller than the cell bodies as visualized in Fig. 2*A*, were then correlated with the positions of

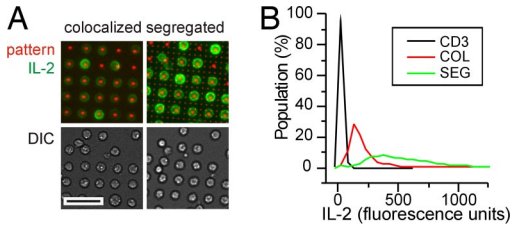

Fig. 3. Modulation of IL-2 secretion. (*A*) IL-2 secretion (green) over 6 h was measured on a cell-by-cell basis. Patterns of anti-CD3 and anti-CD28 antibodies are shown in red. (Scale bar: 25 μm.) (*B*) Histogram of IL-2 secretion from a representative experiment. IL-2 secretion on each of these conditions is statistically different from the other two (both ANOVA and Kruskal–Wallis analysis, $\alpha = 0.01$).

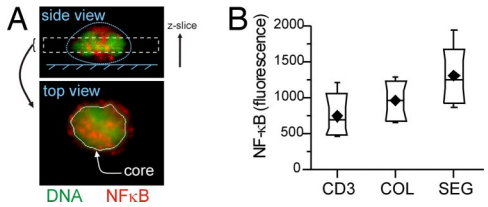

Fig. 4. Modulation of NF-κB translocation. (*A*) NF-κB within the core of the nucleus was measured by segmentation of an image stack. (*B*) Box plots of average NF-κB in the cell nucleus. The whiskers and elements of the boxes correspond to 5, 25, 50, 75, and 95 percentiles of the data, whereas the diamond corresponds to the dataset average. Each condition is statistically different from the other two ($\alpha = 0.01$).

anti-CD28 features. Three representative graphs of the number of anti-CD28 features in contact with an individual cell as a function of time are shown in Fig. 2*C Upper*, and a histogram of fraction of time (frames/total frames) that individual cells were in contact with a specific number of features (mean ± SD, n = 12 cells from a representative experiment) is presented in Fig. 2*C Lower*. Cells were predominantly in contact with three or four features, as desired for our design.

Costimulation Geometry Modulates IL-2 Secretion. IL-2 secretion was measured by using a surface-capture technique in which IL-2 released by a cell is captured and detected on the cell surface, providing a cell-by-cell, spatially resolved measure of IL-2 secretion (Fig. 3*A*). IL-2 secretion was 2- to 3-fold higher on SEG compared with COL patterns (Fig. 3*B*). IL-2 secretion on CD3-only surfaces was smaller than on COL (factor of 15), demonstrating the need for costimulatory signals other than provided by ICAM-1 for naïve T cells. These conditions are statistically different from each other, as determined by both ANOVA and Kruskal–Wallis methods ($\alpha = 0.01, n > 1{,}000$ cells per surface).

Alignment between the anti-CD3 and anti-CD28 features on the SEG surfaces had only a minor effect on IL-2 secretion. Our surfaces exhibit a gradual phasing in which one region contains well separated anti-CD3 and anti-CD28 features (Fig. 1*B*), while hundreds of micrometers away, individual anti-CD28 dots overlapped with a larger anti-CD3 feature. However, our microscopy-based analysis allowed correlation of IL-2 secretion with the geometry of anti-CD3 and anti-CD28 ligands on the underlying surface. Although average IL-2 secretion by cells on well separated patterns was typically 10% higher than on overlapping features, these groups were not consistently statistically different ($\alpha = 0.05$, n = 700–3,000 cells per group), suggesting that the presentation pattern of CD28 may have a larger impact on cell response than registration/segregation from the TCR signal, an aspect that will be revisited later in this study.

NF-κB Translocation. CD28-mediated costimulation contributes to IL-2 production by both transcriptional activation and mRNA stabilization (22–24), with transcription being dependent on translocation of NF-κB from the cytosol to the cell nucleus (25). To determine whether NF-κB is involved in sensing the pattern of CD28 engagement, we imaged nuclear p65 subunit by 3D fluorescence microscopy (Fig. 4*A*). NF-κB translocation, measured as fluorescence intensity within the core of the nucleus, followed that of IL-2 secretion (Fig. 4*B*) and was significantly different between all patterns ($\alpha = 0.01, n > 80$ on each surface). The ability of T cells to discriminate between the SEG and COL patterns is thus driven in part by processes upstream of NF-κB translocation.

PKCθ Recruitment. We then focused on PKCθ recruitment, which is implicated in NF-κB activation and is specifically recruited to the IS (18–20, 26–29). Immunochemical staining for PKCθ in cells fixed at time points from 30 min to 4 h revealed a similar localization across the COL and SEG surfaces, with PKCθ areas overlying anti-CD3 (Fig. 5). A minor, diffuse distribution of PKCθ in proximal areas surrounding these features was also observed. PKCθ clusters were also occasionally observed on features of anti-CD28 (without anti-CD3) but were less prominent than those on the anti-CD3 features. These results suggest that PKCθ recruitment is not involved in distinguishing between the COL and SEG patterns. A similar distribution was observed on the CD3 pattern, but cells withdrew from these surfaces over several hours (outlines in Fig. 5), suggesting a weaker interaction in the absence of CD28 signaling.

Akt Signaling. PKB/Akt is involved in the control of T cell survival, growth, NF-κB activation, and IL-2 mRNA stability (30–33). Activity depends on the association of this protein with the cell membrane but also involves the release of phosphorylated Akt to allow interaction with downstream molecules; immunochemical staining provides only a limited view into Akt activity. Instead, we took a pharmacological approach to examining the role of this pathway, carrying out the IL-2 secretion assay in the presence of triciribene, an Akt inhibitor that does not affect upstream molecules such as PI3K and PDK (34, 35). IL-2 secretion on COL and SEG patterns was reduced in the presence of this inhibitor (Fig. 6*A*). These inhibited levels were higher than on the CD3 surfaces ($\alpha = 0.01$)—indicating that CD28 signaling was not completely inhibited—and similar to each other (no difference observed at $\alpha = 0.05$).

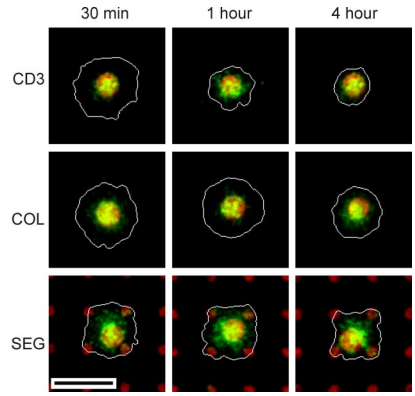

Fig. 5. PKCθ localization is similar across patterns. Patterned antibodies are shown in red, and PKCθ is shown in green. Cell outlines at the substrate interface were generated from long-exposure images and are indicated by dotted lines. (Scale bar: 7 μm.)

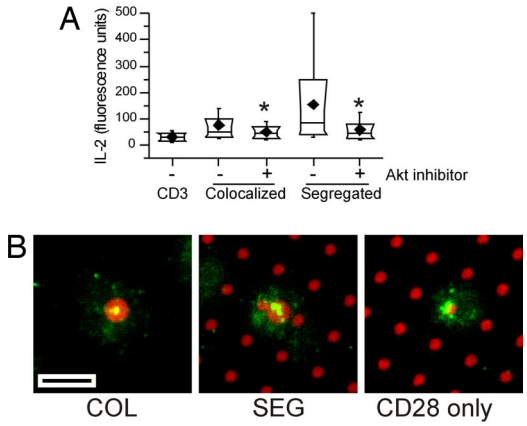

Fig. 6. Inhibition of Akt. (*A*) Six-hour secretion of IL-2 in the presence of the Akt-inhibitor triciribene. No significant difference was detected between experiments indicated by asterisks ($\alpha = 0.05$). All other comparisons indicated significant differences ($\alpha = 0.01$). (*B*) PI3K (green, showing p85α,β subunits) distribution on colocalized and segregated patterns. Patterns of anti-CD3 and anti-CD28 ligands are shown in red. Cells were fixed 10 min after seeding. (Scale bar: 5 μm.)

Like many elements of T cell signaling, CD28 and Akt interact not directly but through the activity of other proteins. To identify a mechanism for modulating Akt, we examined PI3K, which can interact with CD28 and convert PIP_2 to PIP_3. PIP_3 is required for Akt activation and has a widespread distribution in T-B conjugates (36–38). Changing the distribution of active CD28 complexes may thus alter the extent of PIP_3-rich regions of the lipid membrane. PI3K staining of cells on COL patterns indicated small, bright clusters over the anti-CD3/CD28 features. On SEG patterns, these clusters were also localized over the central anti-CD3 feature, with minimal association with the anti-CD28 dots, similar to that on COL patterns, suggesting that this route is not recognition of these patterns. PI3K clusters also occasionally associated with the anti-CD28 dots in cells not in contact with anti-CD3 features (Fig. 6*B*).

Correlation with CD28 Geometry. Finally, we examined two additional variations on the "standard" patterns, which are observed rarely in T-APC conjugates, but are useful in hypothesis testing. The first, a "reverse segregated" pattern, consisted of a central 2-μm feature of anti-CD28 surrounded by 1-μm dots of anti-CD3 (Fig. 7*A*). Cells attached to anti-CD3, typically interacting with three, but sometimes four, individual features. IL-2 secretion (counting only cells that also covered an anti-CD28 feature) was significantly decreased compared with the SEG pattern but higher than on the COL surface (Fig. 7*B*, $\alpha = 0.01$). The second pattern was a "reversed colocalized" configuration of 1-μm dots spaced at 4-μm intervals and containing both anti-CD3 and anti-CD28; unlike the overlapped SEG patterns described earlier, each anti-CD28 feature also contained anti-CD3. IL-2 secretion by cells on this surface was slightly higher than that observed on the SEG pattern making reverse colocalized the most potent pattern (Fig. 7*B*, $\alpha = 0.05$).

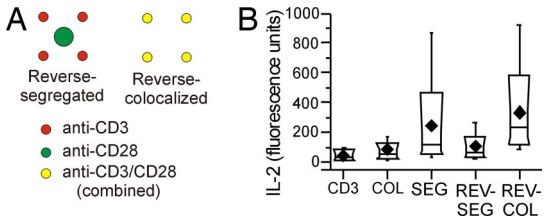

Fig. 7. IL-2 secretion correlates primarily with CD28 geometry. (*A*) Additional geometries of anti-CD3 and anti-CD28 ligands. (*B*) Six-hour IL-2 secretion on these patterns. Data from each pattern are different from all other conditions (Kruskal–Wallis analysis, $\alpha = 0.05$).

Discussion

We demonstrate that the organization of TCR and CD28 signaling in the IS can modulate IL-2 secretion by naïve $CD4^+$ T cells. This report began with the hypothesis that segregation of CD28 from TCR clusters was responsible for the potent costimulatory effect of full-length CD80 observed in a T-APC system (9). However, our results indicate that this effect is more directly related to the change of CD28 signaling. Presentation of anti-CD28 as a pattern of peripheral clusters, rather than a cSMAC-like cluster, enhances IL-2 production; in comparison, changing the geometry of anti-CD3 either within the IS or with respect to anti-CD28 had a smaller, secondary effect. The ability to arbitrarily control the geometry of these signaling components was important in developing these results and is broadly applicable to a range of cellular systems. Interfaces between dendritic cells and T cells often exhibit a multifocal distribution of TCR complexes, segregated from LFA-1/ICAM-1 (39). In a parallel study, CD80 was also found to be multifocal (S.-Y. Tseng, J. C. Waite, M. Liu, and M.L.D., unpublished work), suggesting that dendritic cells, highly effective T cell stimulators, may use the layout of CD28 within the IS as part of the language of cell–cell communication.

Identification of signaling pathways that are modulated in response to IS geometry, along with mechanisms responsible for this control, is important for understanding the functional impacts of spatial organization. We determined that the ability of T cells to discriminate the SEG and COL patterns correlates with NF-κB translocation. In addition, inhibition of the Akt pathway reduced IL-2 secretion on the two patterns to levels that were higher than on CD3 alone and similar to each other (Fig. 6*A*), suggesting that Akt signaling is important in discriminating between the patterns. However, the upstream mechanisms underlying this effect, as well as the exact role that Akt has in these processes, remain unclear. In particular, both PKCθ and PI3K localized to regions of anti-CD3 on both SEG and COL arrays, suggesting that these proteins are not involved in recognition of these patterns. Localization of PI3K to the CD3 regions was unexpected, given the presence of a docking site for this protein on CD28. The association of PKCθ with anti-CD3 was also unexpected because in the T-APC system in which TCR and CD28 clusters appear segregated, PKCθ is robustly recruited to CD28/CD80 clusters (9). Our current results do agree with those of Doh and Irvine (13) for preactivated cells on anti-CD3, however, suggesting that the use of an immobilized, activating antibody rather than cell-bound, peptide-loaded MHC influences PKCθ localization; whereas the use of activating antibodies to drive T cell function is well established, the functional differences between these and physiological ligands are not well understood.

Alternatively, these observations may be related to the spatial dynamics of signaling. Whereas the immobilized antibodies provide good spatial definition of receptor ligation (at a level not typically achievable at the cell–cell interface), downstream signaling molecules are often free to leave the receptor location (40). Immobilized sites of CD28 activation may serve as docking sites of PKCθ to the membrane, which subsequently shed and migrate to regions of TCR activity; although highly speculative, this would be consistent with PKCθ localization to CD28 in the presence of low, background levels of activated TCR on an APC surface and the lack of strong PKCθ localization on the anti-CD28-only regions of Fig. 5. A similar dynamic may influence localization of PI3K and indeed explain the switch of localization shown in Fig. 6*B*. Furthermore, although it has been thought that

PKCθ acts locally, the observation that NF-κB activation sites are scattered in the cytoplasm suggests that the active component of PKCθ may also need to interact transiently with surface receptors and then dissociate to activate downstream targets (41).

Although the use of patterned antibodies to direct receptor location offers several advantages, it does not capture the lateral mobility of receptor complexes on the cell surface that are involved in synapse maturation and modulation of activity of signaling complexes. However, our results suggest that antibody-based activation is more dynamic than may be anticipated from the relatively high affinities of these interactions. On the SEG patterns, cells repeatedly contacted and released features of anti-CD28 (Fig. 2*C*), potentially leading to the generation of new, active sites of CD28 signaling that continually refresh this pathway. This behavior was not seen on the COL surfaces, because the anti-CD3 signal, although present at a lower concentration than anti-CD28, is not as readily released. This could also explain the relatively small impact of moving the anti-CD3 sites to the cell periphery. Finally, the ability of cells to break contacts with anti-CD28 suggests a role of force generation in signaling; the pSMAC region is active and rich in cytoskeletal elements (42, 43). The role of TCR/MHC and CD28/CD80 mobility, including migration to the cSMAC structure, remains an open question.

Methods

Substrate Preparation. Activating antibodies against CD3 (145-2C11) and CD28 (37.51) were purchased from eBioscience. TS2/4 antibody was from American Type Culture Collection. Glass coverslips were cleaned by immersion into hot detergent (Linbro 7X, diluted 1:3 with deionized water), rinsed with MilliQ-grade water, and then baked at 450°C for 6 h. For microcontact printing, topological masters were made by ebeam lithography with a 1-μm PMMA layer, spin-coated onto silicon wafers. Poly(dimethylsiloxane) stamps were cast from these masters (44, 45) and coated, in this hydrophobic state, with antibodies for 30 min, rinsed with PBS, PBS plus 0.05% Tween-20, and deionized water, and then placed in contact with the cleaned coverslips for 1 min. Substrates were rinsed extensively with PBS and then coated with ICAM-1 (as a chimeric fusion with an Fc domain; R&D Systems) at 2 μg/ml for 2 h. These patterns were stable throughout these experiments and in fact can last up to several weeks (17). To estimate the surface concentrations of these proteins, a fraction of the antibodies were labeled with Texas red before patterning onto substrates. Fluorescence intensities of these structures were compared against a series of supported lipid bilayers consisting of egg PC (Avanti Polar Lipids) supplemented with specific concentrations (0.03–0.14 mol %) of Texas red-DHPE (Invitrogen) (17, 46); these bilayers provide a consistent, uniform set of concentration standards (a figure of 3.3×10^6 lipids per μm^2 of bilayer was used in this study).

T Cells. $CD4^+$ T cells were isolated from lymph nodes of C57BL/6 mice by negative selection (Dynal CD4 Negative Isolation Kit from Invitrogen). Naïve T cells comprised typically >85% of the cell population, as quantified by cells exhibiting a combination of high/low levels of CD44/CD62L, respectively. For experiments, cells were resuspended in RPMI medium 1640 (Invitrogen) plus 5% mouse serum and seeded onto the micropatterned substrates at a density of 2×10^4 cells per mm^2 immediately after isolation.

Immunochemistry. For observation of protein localization, cells were fixed and extracted by using 4% paraformaldehyde plus 0.25% Triton X-100 (4°C) and then stained by using standard immunofluorescence techniques. Polyclonal antibodies for PKCθ (product code sc-212; c-terminus), NF-κB (sc-109; p65 subunit), and PI3K (sc-423; p85 subunit) were purchased from Santa Cruz Biotechnology. Cells were counterstained by using the SYTOX Green DNA dye (Invitrogen) before visualization.

IL-2 Assays. Immediately before seeding, cells were incubated with an IL-2 capture reagent from a secretion assay kit (Miltenyi Biotec). One hour after seeding, samples were gently rinsed with warm (37°C) RPMI medium 1640. After 6 h (total) of incubation (37°C), cells were rinsed and incubated with a fluorescently labeled antibody to IL-2. The average fluorescence intensity associated with APC-labeled IL-2 was estimated by microscopy on a cell-by-cell basis. *Akt* inhibition experiments were carried out by including triciribine (Calbiochem) in the culture media at a concentration of 10 μM.

Statistics. Data were analyzed by using Kruskal–Wallis approaches. When presented as box plots, the whiskers and box elements correspond to 5, 25, 50, 75, and 95 percentiles. All samples from a single experiment were processed in one session, and statistical comparisons were made only within a single experiment. Experiments were carried out at least three times to establish consistency.

ACKNOWLEDGMENTS. This article and the project described were supported in part by National Institutes of Health, EB008199 and EY016586. The latter is part of the NIH Roadmap for Medical Research. Additional support was provided by the Whitaker Foundation (through a Special Development Award to Columbia University).

1. Bromley SK, *et al.* (2001) The immunological synapse. *Annu Rev Immunol* 19:375–396.
2. Friedl P, den Boer AT, Gunzer M (2005) Tuning immune responses: Diversity and adaptation of the immunological synapse. *Nat Rev Immunol* 5:532–545.
3. Grakoui A, *et al.* (1999) The immunological synapse: A molecular machine controlling T cell activation. *Science* 285:221–227.
4. Davis MM, *et al.* (2003) Dynamics of cell surface molecules during T cell recognition. *Annu Rev Biochem* 72:717–742.
5. Groves JT, Dustin ML (2003) Supported planar bilayers in studies on immune cell adhesion and communication. *J Immunol Methods* 278:19–32.
6. Krummel MF, Macara I (2006) Maintenance and modulation of T cell polarity. *Nat Immunol* 7:1143–1149.
7. Kupfer A (2006) Signaling in the immunological synapse: Defining the optimal size. *Immunity* 25:11–13.
8. Andres PG, *et al.* (2004) CD28 signals in the immature immunological synapse. *J Immunol* 172:5880–5886.
9. Tseng S-Y, Liu M, Dustin ML (2005) CD80 cytoplasmic domain controls localization of CD28, CTLA-4, and Protein Kinase C-θ in the immunological synapse. *J Immunol* 175:7829–7836.
10. Doty RT, Clark EA (1996) Subcellular localization of CD80 receptors is dependent on an intact cytoplasmic tail and is required for CD28-dependent T cell costimulation. *J Immunol* 157:3270–3279.
11. Bromley SK, *et al.* (2001) The immunological synapse and CD28-CD80 interactions. *Nat Immunol* 2:1159–1166.
12. Mossman KD, Campi G, Groves JT, Dustin ML (2005) Altered TCR signaling from geometrically repatterned immunological synapses. *Science* 310:1191–1193.
13. Doh J, Irvine DJ (2006) Immunological synapse arrays: Patterned protein surfaces that modulate immunological synapse structure formation in T cells. *Proc Natl Acad Sci USA* 103:5700–5705.
14. Whitesides GM, Ostuni E, Takayama S, Jiang X, Ingber DE (2001) Soft lithography in biology and biochemistry. *Annu Rev Biomed Eng* 3:335–373.
15. Chen CS, Mrksich M, Huang S, Whitesides GM, Ingber DE (1998) Micropatterned surfaces for control of cell shape, position, and function. *Biotechnol Prog* 14:356–363.
16. Kumar A, Whitesides GM (1993) Features of gold having micrometer to centimeter dimensions can be formed through a combination of stamping with an elastomeric stamp and an alkanethiol ''ink'' followed by chemical etching. *Appl Phys Lett* 63:2002.
17. Shi P, Shen K, Kam L (2007) Local presentation of L1 and N-cadherin in multicomponent, microscale patterns differentially direct neuron function in vitro. *Dev Neurobiol* 67:1765–1776.
18. Schmitz ML, Krappmann D (2006) Controlling NF-κB activation in T cells by costimulatory receptors. *Cell Death Differ* 13:834–842.
19. Weil R, Israël A (2006) Deciphering the pathway from the TCR to NF-κB. *Cell Death Differ* 13:826–833.
20. Sims TN, *et al.* (2007) Opposing effects of PKCθ and WASp on symmetry breaking and relocation of the immunological synapse. *Cell* 129:773–785.
21. Dustin ML, Bromley SK, Kan Z, Peterson DA, Unanue ER (1997) Antigen receptor engagement delivers a stop signal to migrating T lymphocytes. *Proc Natl Acad Sci USA* 94:3909–3913.
22. June CH, *et al.* (1989) Two distinct mechanisms of interleukin-2 gene expression in human T lymphocytes. *J Autoimmun* 2(Suppl):55–65.
23. Sanchez-Lockhart M, *et al.* (2004) Cutting edge: CD28-mediated transcriptional and posttranscriptional regulation of IL-2 expression are controlled through different signaling pathways. *J Immunol* 173:7120–7124.
24. Sanchez-Lockhart M, Miller J (2006) Engagement of CD28 outside of the immunological synapse results in up-regulation of IL-2 mRNA stability but not IL-2 transcription. *J Immunol* 176:4778–4784.
25. Ghosh P, Tan TH, Rice NR, Sica A, Young HA (1993) The interleukin 2 CD28-responsive complex contains at least three members of the NF-κB family: c-Rel, p50, and p65. *Proc Natl Acad Sci USA* 90:1696–1700.
26. Monks CR, Kupfer H, Tamir I, Barlow A, Kupfer A (1997) Selective modulation of protein kinase C-θ during T-cell activation. *Nature* 385:83–86.
27. Altman A, Villalba M (2003) Protein kinase C-theta; (PKCθ): It's all about location, location, location. *Immunol Rev* 192:53–63.
28. Bi K, *et al.* (2001) Antigen-induced translocation of PKC-θ to membrane rafts is required for T cell activation. *Nat Immunol* 2:556–563.

29. Sun Z, *et al.* (2000) PKC-θ is required for TCR-induced NF-κB activation in mature but not immature T lymphocytes. *Nature* 404:402–407.
30. Kane LP, Andres PG, Howland KC, Abbas AK, Weiss A (2001) Akt provides the CD28 costimulatory signal for up-regulation of IL-2 and IFN-γ but not TH2 cytokines. *Nat Immunol* 2:37–44.
31. Frauwirth KA, *et al.* (2002) The CD28 signaling pathway regulates glucose metabolism. *Immunity* 16:769–777.
32. Jones RG, *et al.* (2005) NF-κB couples protein kinase B/Akt signaling to distinct survival pathways and the regulation of lymphocyte homeostasis in vivo. *J Immunol* 175:3790–3799.
33. Pei Y, *et al.* (2008) Nuclear export of NF90 to stabilize IL-2 mRNA is mediated by AKT-dependent phosphorylation at Ser647 in response to CD28 costimulation. *J Immunol* 180:222–229.
34. Karst AM, Dai DL, Cheng JQ, Li G (2006) Role of p53 up-regulated modulator of apoptosis and phosphorylated Akt in melanoma cell growth, apoptosis, and patient survival. *Cancer Res* 66:9221–9226.
35. Yang L, *et al.* (2004) Akt/Protein Kinase B Signaling Inhibitor-2, a selective small molecule inhibitor of Akt signaling with antitumor activity in cancer cells overexpressing Akt. *Cancer Res* 64:4394–4399.
36. Okkenhaug K, Bilancio A, Emery JL, Vanhaesebroeck B (2004) Phosphoinositide 3-kinase in T cell activation and survival. *Biochem Soc Trans* 32:332–335.
37. Parry RV, Riley JL, Ward SG (2007) Signalling to suit function: Tailoring phosphoinositide 3-kinase during T-cell activation. *Trends Immunol* 28:161–168.
38. Costello PS, Gallagher M, Carntrell DA (2002) Sustained and dynamic inositol lipid metabolism inside and outside the immunological synapse. *Nat Immunol* 3:1082–1089.
39. Brossard C, *et al.* (2005) Multifocal structure of the T cell–dendritic cell synapse. *Eur J Immunol* 35:1741–1753.
40. Bunnell SC, *et al.* (2002) T cell receptor ligation induces the formation of dynamically regulated signaling assemblies. *J Cell Biol* 158:1263–1275.
41. Schaefer BC, Kappler JW, Kupfer A, Marrack P (2004) Complex and dynamic redistribution of NF-κB signaling intermediates in response to T cell receptor stimulation. *Proc Natl Acad Sci USA* 101:1004–1009.
42. Campi G, Varma R, Dustin ML (2005) Actin and agonist MHC-peptide complex-dependent T cell receptor microclusters as scaffolds for signaling. *J Exp Med* 202:1031–1036.
43. Kaizuka Y, Douglass AD, Varma R, Dustin ML, Vale RD (2007) Mechanisms for segregating T cell receptor and adhesion molecules during immunological synapse formation in Jurkat T cells. *Proc Natl Acad Sci USA* 104:20296–20301.
44. Odom TW, Love JC, Wolfe DB, Paul KE, Whitesides GM (2002) Improved pattern transfer in soft lithography using composite stamps. *Langmuir* 18:5314–5320.
45. Schmid H, Michel B (2000) Siloxane polymers for high-resolution, high-accuracy soft lithography. *Macromolecules* 33:3042–3049.
46. Kung LA, Kam L, Hovis JS, Boxer SG (2000) Patterning hybrid surfaces of proteins and supported lipid bilayers. *Langmuir* 16:6773–6776.